DEPARTMENT OF MECHANICAL ENGINEERING
COLLEGE OF ENGINEERING & TECHNOLOGY
OLD DOMINION UNIVERSITY
NORFOLK, VIRGINIA 23529

INVESTIGATION OF HIGH-SPEED FREE SHEAR FLOWS USING IMPROVED PRESSURE-STRAIN CORRELATED REYNOLDS STRESS TURBULENCE MODEL

By

B. Lakshmanan, Research Associate

and

S.N. Tiwari, Principal Investigator

Supplemental Progress Report
For the period ended August 1991

Prepared for
National Aeronautics and Space Administration
Langley Research Center
Hampton, VA 23681-0001

Under
Research Grant NAG-1-423
Dr. A. Kumar, Technical Monitor
FLDMD-Theoretical Flow Physics Branch

November 1993

DEPARTMENT OF MECHANICAL ENGINEERING
COLLEGE OF ENGINEERING & TECHNOLOGY
OLD DOMINION UNIVERSITY
NORFOLK, VIRGINIA 23529

INVESTIGATION OF HIGH-SPEED FREE SHEAR FLOWS USING IMPROVED PRESSURE-STRAIN CORRELATED REYNOLDS STRESS TURBULENCE MODEL

By

B. Lakshmanan, Research Associate

and

S.N. Tiwari, Principal Investigator

Supplemental Progress Report
For the period ended August 1991

Prepared for
National Aeronautics and Space Administration
Langley Research Center
Hampton, VA 23681-0001

Under
Research Grant NAG-1-423
Dr. A. Kumar, Technical Monitor
FLDMD-Theoretical Flow Physics Branch

Submitted by the
Old Dominion University Research Foundation
P.O. Box 6369
Norfolk, Virginia 23508-0369

November 1993

FOREWORD

This is a supplemental progress report on the research project, "Analysis and Computation of Internal Flow-Field in a Scramjet Engine," for the period ended August 1991. Certain modifications were made in the analysis and computational procedures during 1992 after receiving inputs from the professional communities at national conferences. The manuscript was prepared, in the final form, during the summer of 1993.

The authors are indebted to Mr. Sutanu Sarkar of the Institute for Computer Applications in Science and Engineering (ICASE) at NASA Langley Research Center for his cooperation and technical assistance. Partial funding for this research was provided by the NASA Langley Research Center through the Grant NAG-1–423. The grant was monitored by Dr. Ajay Kumar of Theoretical Flow Physics Branch (Fluid Mechanics Division), Mail Stop 156, NASA Langley Research Center, Hampton, Virginia 23681–0001.

INVESTIGATION OF HIGH-SPEED FREE SHEAR FLOWS USING IMPROVED PRESSURE-STRAIN CORRELATED REYNOLDS STRESS TURBULENCE MODEL

B. Lakshmanan[‡] and S. N. Tiwari[§]
Department of Mechanical Engineering and Mechanics
Old Dominion University, Norfolk, VA 23529–0247

ABSTRACT

A high-speed shear layer is studied using compressibility corrected Reynolds stress turbulence model which employs newly developed model for pressure-strain correlation. MacCormack explicit prediction-corrector method is used for solving the governing equations and the turbulence transport equations. The stiffeness arising due to source terms in the turbulence equations is handled by a semi-implicit numerical technique. Results obtained using the new model show a sharper reduction in growth rate with increasing convective Mach number. Some improvements were also noted in the prediction of the normalized streamwise stress and Reynolds shear stress. The computed results are in good agreement with the experimental data.

‡ Research Associate
§ Eminent Professor

TABLE OF CONTENTS

LIST OF FIGURES

LIST OF SYMBOLS

F	Vector representing the x-component of the distruction and redistribution of the Reynolds stresses in Eq. (3.1)
G	Vector representing the y- component of the distruction and redistribution of the Reynolds stresses in Eq. (3.1)
H	Source term vector in Eq. (3.1)
J	Jacobian of the coordinate transformation
k	Turbulent Kinetic energy
M	Mach number
p	Static pressure
R	Gas constant
T	Static temperature
t	time
U	Vector of conserved variables
u,v	Velocity components in x and y direction
x,y	Cartesian coordinates

Greek Symbols

ϵ	Dissipation of turbulent kinetic energy
γ	Ratio of specific heats
δ	Shear layer thickness
Δt	Time step in Eqs. 3.2 and 3.3
ξ, η	Computational coordinates
ρ	Density

Subscripts

1	Primary stream
2	Secondary stream
∞	Freestream

1. INTRODUCTION

The recent resurging interest in a High Speed Civil Transport (HSCT) and the National Aerospace Plane (NASP) clearly demonstrates the need for advanced propulsion systems for supersonic velocities and beyond. Because of the complex nature of the problem, numerous research programs have been initiated. One aspect of this research has been directed towards detailed understanding of the complex flowfield in the engine over a wide range of operating conditions. Computational fluid dynamics (CFD) in conjunction with recent advances in turbulence modeling is used extensively for detailed investigation of the engine flowfield, as existing wind tunnel facilities are inadequate especially in the high Mach number regime. Because of the complex nature of the flowfield and increased computational resources necessary, detailed simulation of the complete engine problem cannot be considered at the present time. A more tractable problem that can be considered in isolation of the complexities introduced by the engine geometry is posed by the spatially evolving mixing layer. Currently there is a renewed interest in compressible mixing layers for two main reasons. First, mixing layers play an important role in many engineering applications, as they are central to many advanced propulsion systems. This stems from the fact that they govern the rate of mixing in combustion chambers and are also responsible for most of the acoustic noise generated by many propulsion systems. Apart from its practical applications, the compressible shear layer problem has remained as the most celebrated case for basic testing of transport equation turbulence models.

It is known that variable density extensions of standard incompresible turbulence models [1,2] are inadequate in duplicating the experimentally observed [3,4] reduction in growth rate with increasing convective Mach number. This led to attempts by Oh [5], Vandromme [6], and Dussage and Quine [7], among others to make modifications to incompressible turbulence models in order to obtain successful prediction of the compressible mixing layer. But these modifications were developed somewhat on a preliminary fashion and lack the theoretical justifications necessary to model the physics of the flow adequately when parameters beyond mean growth

rates are considered. Recently, Sarkar et al. [8,9] recognized the importance of compressible dissipation and pressure-dilatation which are known to be present in compressible turbulence. Simple corrections for compressible dissipation and pressure-dilatation were proposed based on direct numerical simulation of compressible isotropic turbulence which can be easily included in the existing transport equation turbulence models. In addition, Speziale et al. [10] recently developed a new model for pressure-strain correlation which was shown to give improved predictions over older models such as the Launder, Reece and Rodi model [2] when applied to incompressible, homogeneous turbulent flows.

During the past decade, considerable progress have been made in the area of computational fluid dynamics. Most of the research activities have been centered around computing complex three-dimensional flows over realistic aerodynamic configurations. Despite the popularity of the existing schemes in computing complex flows, their extension for solving stiff equations are limited in the literature, especially within the framework of full Navier-Stokes solvers.

Recently, Sarkar and Lakshmanan [11] applied the compressibility corrected Reynolds stress turbulence model [2] to high speed shear layer using a full Navier-Stokes code. While the numerical study was successful, the components of the Reynolds stress were overpredicted. The purpose of the study is to incorporate the newly developed pressure-strain correlation in the compressibility corrected Reynolds stress model [11]. The resulting turbulence model is then applied to the case of high-speed shear layer over a wide range of convective Mach number.

2. THEORETICAL FORMULATION

In this section, essential governing equations, and boundary and initial conditions are presented for a compressible supersonic mixing layer evolving downstream of a splitter plate (Fig. 2.1).

2.1 Governing Equations

The formulation of the problem starts with the Favre-averaged form of the equations representing conservation of mass, momentum, energy and turbulence quantities. The overbar is used to denote a conventional Reynolds average, whereas the tilde is used to denote the Favre-average. For the sake of brevity only the Reynolds stress and dissipation rate transport equations are given here. Extensive details of the governing equations and models are given in Ref. [11].

Reynolds Stress Equation

$$\frac{\partial}{\partial t}\left(\bar{\rho}\,\widetilde{u_i'u_j'}\right)+\frac{\partial}{\partial x_k}\left[\bar{\rho}\tilde{u}_k\widetilde{u_i'u_j'}+T_{ijk}+\left(\delta_{ik}\overline{p''u_j''}+\delta_{jk}\overline{p''u_i''}\right)-\left(\overline{S_{ik}''u_j''}+\overline{S_{jk}''u_i''}\right)\right]=P_{ij}+\Pi_{ij}-\frac{2}{3}\bar{\rho}\left(\tilde{\epsilon}_s+\tilde{\epsilon}_c\right)+\frac{2}{3}\overline{p''u_{k,k}''}\,\delta_{ij}-\left(u_i'\frac{\partial\bar{p}}{\partial x_j}+\overline{u_j'}\,\frac{\partial\bar{p}}{\partial x_i}\right) \tag{2.1}$$

where P represents production, Π is the pressure-strain correlation and T_{ijk} is the diffusive transport. The third and fourth term inside the square bracket on the LHS represents the contribution due to pressure-velocity and stress-velocity correlations respectively. In the present work these correlations are neglected. The third and fourth terms on the RHS represents the contribution due to compressible dissipation and pressure-dilatation effects. In the present work, these terms are computed using the Sarkar's model [8,9]. In Eq. (2.1), the production tensor P_{ij} is defined in an exact manner while models are carried for the remaining terms.

Production Tensor P_{ij}:

$$P_{ij}=-\bar{\rho}\left(\widetilde{u_i'u_k'}\,\tilde{u}_{j,k}+\widetilde{u_j'u_k'}\,\tilde{u}_{i,k}\right) \tag{2.2}$$

Model for Diffusive Transport:

$$T_{ijk} = -C_s\bar{\rho}\,\frac{\left(\widetilde{q^2}\right)^2}{\tilde{\epsilon}_s}\left[\left(\widetilde{u_i'u_j'}\right)_{,k} + \left(\widetilde{u_j'u_k'}\right)_{,i} + \left(\widetilde{u_i'u_k'}\right)_{,j}\right] \tag{2.3}$$

where $\widetilde{q'^2} = \widetilde{u'^2} + \widetilde{v'^2} + \widetilde{w'^2}$ and the model constant C_s = 0.018.

Model for Compressible Dissipation

$$\tilde{\epsilon}_c = \alpha_1\,\tilde{\epsilon}_s M_t^2 \tag{2.4}$$

Model for Pressure-Dilatation:

$$\overline{p''u''_{k,k}} = -\alpha_2\bar{\rho}P_{ij}M_t^2 + \alpha_3\bar{\rho}\tilde{\epsilon}_s M_t^2$$

where $M_t = \sqrt{\dfrac{\tilde{q}^2}{\gamma R\tilde{T}}}$ is the turbulent Mach number and $\tilde{\varepsilon}_s$ is the solenoidal dissipation. Based on direct numerical simulation Sarkar [8,9] recommends α_1 = 0.5, α_2 = 0.4 and α_3=0.2.

Model for Pressure-Strain Correlation

Two models are employed in the present study for pressure-strain correlation. The first model employs the well known Launder, Reece and Rodi model [2] while the second model employs the recently developed SSG model [9]. The details of the model are given as follows:

Original Pressure-Strain Correlation Model [2]:

$$\Pi_{ij} = -C_1\bar{\rho}\,\tilde{\epsilon}_s b_{ij} - C_2\left(P_{ij} - \frac{P_{kk}}{3}\,\delta_{ij}\right) \tag{2.5}$$

where b_{ij} is the anisotropy tensor given by

$$b_{ij} = \frac{\widetilde{u_i'u_j'}}{\tilde{q}^2} - \frac{\delta_{ij}}{3} \tag{2.6}$$

In Eq. (2.6), the model constants are C_1 = 3.0 and C_2 = 0.6

Improved Pressure-Strain Correlation Model [9]:

$$\begin{aligned} II_{ij} &= -(C_3\tilde{\epsilon}_s + C_3^*P)b_{ij} + C_4\tilde{\epsilon}_s\left(b_{ik}b_{kj} - \frac{1}{3}b_{mm}b_{mn}\delta_{ij}\right) \\ &+ \left(C_5 - C_5^* II^{1/2}\right)\tilde{k}\left(\tilde{S}_{ij} - \frac{1}{3}\tilde{S}_{kk}\delta_{ij}\right) + C_6\,\tilde{k}\,\left(b_{ik}\tilde{S}_{jk} + b_{jk}\tilde{S}_{ik}\right. \\ &\left. - \frac{2}{3}b_{mn}\tilde{S}_{mn}\delta_{ij}\right) + C_7\tilde{k}\left(b_{ik}\tilde{W}_{jk} + b_{jk}\tilde{W}_{ik}\right) \end{aligned} \tag{2.7}$$

$$\tilde{S}_{ij} = \frac{1}{2}(\tilde{u}_{i,j} + \tilde{u}_{j,i}) \ , \ \tilde{W}_{i,j} = \frac{1}{2}(\tilde{u}_{i,j} - \tilde{u}_{j,i}) \tag{2.8}$$

$$\mathrm{P} = -\tau_{ij} \ \widetilde{u}_{i,j} \ , \quad \mathrm{II} = b_{ij} b_{ij} \tag{2.9}$$

The model constants are

$$\mathrm{C}_3 = 3.4 \ , \quad \mathrm{C}_3^* = 1.8 \ , \quad \mathrm{C}_4 = 4.2$$

$$\mathrm{C}_5 = 0.8 \ , \quad \mathrm{C}_5^* = 1.3 \ , \quad \mathrm{C}_6 = 1.25 \ , \quad \mathrm{C}_7 = 0.4$$

The new models for compressible dissipation, pressure-dilatation and pressure-strain correlation were chosen because these models have been developed based on direct numerical simulation of homogeneous isotropic turbulence.

Dissipation Transport Equation

The dissipation transport equation is expressed as

$$\frac{\partial}{\partial t}(\bar{\rho}\,\widetilde{\epsilon}_s) + \frac{\partial}{\partial x_k}\left[\bar{\rho}\,\tilde{u}_k\tilde{\epsilon}_s - C_\epsilon \frac{\bar{\rho}\tilde{k}}{\tilde{\epsilon}_s}\,\widetilde{u_k' u_l'}\,\frac{\partial \widetilde{\epsilon}_s}{\partial l}\right] = -C_{\epsilon 1}\frac{\tilde{\epsilon}_s}{\tilde{k}}\bar{\rho}\,\widetilde{u_i' u_j'}\frac{\partial \tilde{u}_i}{\partial x_j} - C_{\epsilon 2}\frac{\bar{\rho}\,\tilde{\epsilon}_s^{\,2}}{\tilde{k}} \tag{2.10}$$

The model coefficients in Eq. (2.10) are

$$\mathrm{C}_{\epsilon 1} = 1.44 \ , \quad \mathrm{C}_{\epsilon 2} = 1.83 \ , \quad \mathrm{C}_\epsilon = 0.15$$

For the present problem, we need to solve the Navier-Stokes equations along with the equations of state, to obtain the mean variables $\bar{\rho}, \tilde{\mathrm{u}}, \tilde{\mathrm{v}}$ and $\tilde{\mathrm{E}}$. In the case of the plane shear layer, the Reynolds stress tensor has four nonzero component: $\widetilde{u'^2}$, $\widetilde{v'^2}$, $\widetilde{w'^2}$ and $\widetilde{u'v'}$, which are solved by the corresponding components of Eq. (2.1). The equation for the solinoidal dissipation $\tilde{\epsilon}_s$ completes the set of governing equations. Thus, a system of nine coupled, nonlinear, partial differential equations along with an appropriate set of initial and boundary conditions must be solved.

2.2 Boundary and Initial Conditions

Since the governing equations are elliptic in nature, the boundary conditions have to be specified along all four boundaries. These include inflow, outflow, and outer boundaries (lower and upper boundaries), respectively. At the inflow boundary ($x = 0.0$), profiles are specified for the velocities, static pressure, static temperature, turbulent stresses, and the turbulent dissipation rate. Since we are interested in the downstream fully develop regime, the specific form of the inlet profiles is not crucial.

The outer boundaries always remain in the freestream, and the appropriate boundary condition is to assume that the normal derivative of the flow variables vanish along those boundaries. The gradient boundary conditions not only preserve the freestream values along the outer boundaries but also provide nonreflective conditions for the outgoing waves. The outflow boundary ($x = x_{max}$) is always supersonic and, hence, the values of mean flow and turbulence quantities are determined by zeroth-order extrapolation from upstream values. Along with the boundary conditions, the governing equations also require a set of initial conditions. The initial conditions at time $t = 0$ for all of the variables are obtained by simply propagating the inflow profiles throughout the computational domain. Having specified all of the boundary and initial data, the equations are marched in time until the residual based on $\bar{\rho}\,\bar{u}$ decreases by six orders of magnitude, indicating that a converged solution has been obtained.

3. METHOD OF SOLUTION

The transport equations for the mean flow and Reynolds stresses are written in the physical domain and must be transformed to the computational domain using an appropriate coordinate transformation. For the physical problem under consideration, an algebraic grid generation technique is used to generate the mesh. In the physical domain, a uniform grid is used in the axial direction and in the normal direction the grid lines are clustered near regions where strong gradients exist. A uniform mesh is used in the computational domain. The governing equations are first cast into a vector form, where U is the dependent variable vector consisting of nine components; the vectors F and G, respectively, denote the x and y destruction and redistribution of the Reynolds stresses. To numerically obtain the solution for the vector U, the governing equations are then transformed from the physical domain to the computational domain, giving the following system of equations,

$$\frac{\partial \hat{U}}{\partial t} + \frac{\partial \hat{F}}{\partial \xi} + \frac{\partial \hat{G}}{\partial \eta} = \hat{H} \tag{3.1}$$

where

$$\hat{U} = JU, \qquad \hat{H} = JH$$

$$\hat{F} = Fy_\eta - GX_\eta, \quad \hat{G} = Gx_\xi - Fy_\xi, \quad J = x_\xi y_\eta - y_\xi x_\eta$$

In Eq. (3.1), a superscript ($\hat{}$) denotes quantities in the transformed system, $(x_\xi, x_\eta, y_\xi, y_\eta)$ represent the metrics of the transformation, and J denotes the Jacobian of the transformation. If the physical grid is given, the metrics and the Jacobian of the transformation can be computed easily.

The governing equations are integrated explicitly in time using the unsplit MacCormack predictor-corrector scheme [12]. During a specific numerical sweep, the inviscid fluxes and the first-derivative terms in the source vector H are backward differenced in the predictor step and forward differenced in the corrector step. Second-order central differences are used for the viscous and heat flux terms. Hence, the complete scheme for both the predictor and corrector steps can be expressed as follows

Predictor:

$$\Delta\hat{U}_{i,j}^{\overline{n+1}} = -\Delta t\left(\frac{\nabla_\xi \hat{F}_{i,j}^{n}}{\Delta\xi} + \frac{\nabla_\eta \hat{G}_{i,j}^{n}}{\Delta\eta} - \hat{H}_{i,j}^{n}\right) \tag{3.2a}$$

$$\hat{U}_{i,j}^{\overline{n+1}} = \hat{U}_{i,j}^{n} + \Delta\hat{U}_{i,j}^{\overline{n+1}} \tag{3.2b}$$

Corrector:

$$\Delta\hat{U}_{i,j}^{n+1} = -\Delta t\left(\frac{\Delta_\xi \hat{F}_{i,j}^{\overline{n+1}}}{\Delta\xi} + \frac{\Delta_\eta \hat{G}_{i,j}^{\overline{n+1}}}{\Delta\eta} - \hat{H}_{i,j}^{\overline{n+1}}\right) \tag{3.3a}$$

$$\hat{U}_{i,j}^{n+1} = 1/2\left(\hat{U}_{i,j}^{n} + \hat{U}_{i,j}^{\overline{n+1}} + \Delta\hat{U}_{i,j}^{n+1}\right) \tag{3.3b}$$

The composite numerical scheme is second-order accurate in both time and space and, being an explicit scheme, is conditionally restricted by the Courant and viscous stability limits of the governing equations. The solution procedure requires no scalar or block tridiagonal inversions. The flow-field is advanced from time level n to n +1 and this process is continued until the desired integration time or steady state has been reached. Since the Reynolds stress transport equations contain stiff source terms, the maximum Courant-Friedricks-Lewy (CFL) number used in the computation was limited to 0.5.

The numerical code used in this study is a two-dimensional, Navier-Stokes solver [13] written in a generalize body-oriented coordinate system. As such, various two-dimensional free shear flows and wall bounded flows can be handled by the numerical code. The code in its original form used a second-order spatially and temporally accurate two-step MacCormack scheme. The later versions of the code employ a variety of higher order compact algorithms [14] (fourth and sixth order) and various upwind schemes. Local time stepping and residual smoothing options are also available in the code to accelerate the convergence to steady state. In the present research work, the capabilities of the code are further enhanced by adding a second-order Reynolds stress model as a turbulence closure.

4. RESULTS AND DISCUSSION

A shear layer developing due to mixing between parallel supersonic streams in chosen as a test case to validate the newly developed turbulence model. Extensive results have been obtained over a wide range of convective Mach number. These results serve two purposes. First, the numerical procedure and the developed computer code are validated by comparing with the experimental results [4, 15–18]. Secondly, they explain the characteristic behavior of high-speed shear layers. It should be pointed out that all the results reported in this paper are computed without artificial dissipation added to the numerical scheme.

Results were obtained for extensive range of convective Mach number by varying the upper speed U_1 from 900 m/sec to 4000 m/sec while maintaining the lower speed U_2 at 800 m/sec. The static conditions for the two incident streams were assumed to be equal. Specifically the results were obtained for the following conditions:

$$p_\infty = 101325 \text{ N/m}^2, \quad T_\infty = 800 \text{ K}, \rho_\infty = 0.44 \text{ kg/m}^3$$

Computations were carried out for a shear layer (Fig. 2.1) developing over a length of 10 cm. The height of the domain was assumed to be 5 cm. Before discussing the results, a few definitions are in order. It is well known from the experiments that a fully-developed shear layer spreads linearly, and that the growth rate $d\delta/dx$ can be expressed by the following relation:

$$\frac{d\delta}{dx} = C_\delta \left(\frac{u_1 - u_2}{u_1 + u_2} \right) \tag{4.1}$$

where $\delta(x)$ denotes the thickness of the shear layer, and C_δ is approximately constant. The shear layer thickness $\delta(x)$ represents the distance between the two cross-stream locations where the normalized streamwise velocity $u^* = (u - u_2)/(u_1 - u_2)$ is 0.1 and 0.9 respectively. The convective Mach number M_c is defined by the following relationship:

$$M_c = \left(\frac{u_1 - u_2}{a_1 + a_2} \right) \tag{4.2}$$

where a_1 and a_2 are the speeds of sound in the two layers.

The calculations were carried out using 201x51 mesh. A uniformly spaced grid was used in the streamwise direction while a stretched grid was employed in the cross-stream direction. A grid refinement study was carried out in the cross-stream direction for all convective Mach numbers using 101 and 201 points. Grid independent results were obtained between 101 and 201 points and the variation in the solution between 51 and 101 points was found to be less than 1%.

Figures 4.1 – 4.4 show the results obtained using the compressibility corrected form of the original model and the improved model for a particular set of conditions of the shear layer having primary stream velocity $u_1 = 2500^m/_s$.

The velocity and the Reynolds stress profiles were plotted as a function of the similarity variable $\eta = (y - y_c)/\delta$ where y is the normal coordinate and y_c is the normal coordinate location where u^*=0.5.

Figure 4.1 shows that the mixing layer thickness δ(x) increases linearly after an initial development phase. It is evident that at the outflow boundary of the computational domain, the linearly growing regime is well established and the mean velocity profiles have achieved self similar form. The improved model predicts a slightly reduced mixing layer thickness compared to the predictions shown by the original model.

Figures 4.2 – 4.4 show the comparison of the fully developed mean velocity and turbulent stress profiles computed by the two models. These profiles clearly display the asymmetry present in the flow field as shown by the downward movement of the center of the mixing layer (y coordinate location where u^*=0.5) with axial location (Fig. 4.5). The improved model yields slightly reduced peak values for the normal stress and Reynolds shear Stress. These results clearly indicate a greater-penetration of the flow into the low-speed than the corresponding penetration into the upper high-speed side of the domain.

Figure 4.6 shows the normalized growth rate for a fully developed flow ($(C_\delta)_o$ being the incompressible value which was obtained by calculating case with a small M_c) as a function of convective Mach number. It is seen that without compressibility effects (α=0.0) both the models show only a mild decrease in growth rate with increasing convective Mach number. However,

inclusion of the compressibility correction to the models (α=1.0) lead to a sharper reduction in growth rate with increasing convective Mach number. Improved results for the growth rate are obtained using the compressibility corrected form of the new model as compared to the original model especially in the high convective Mach number regime. Figures 4.7 and 4.8 show the computed peak normal stress and Reynolds shear Stress and comparison with the experimental data [4, 16–18]. The peak values of the normalized stress components decrease significantly with increasing convective Mach number. This is thought to be a direct consequence of the compressibility correction which has a dissipative effect on the growth rate of the turbulent kinetic energy and shear stress. It is clear that results obtained using the improved model are well within the range of the experimental data unlike those of the original model.

5. CONCLUSIONS

Initially, a second-order turbulence closure (employing Lauder, Reece and Rodi model for pressure-strain correlation) without any compressibility correction was applied to high-speed shear layer. The results confirmed that variable density extensions of incompressible turbulence models were inadequate in duplicating the experimentally reduction in growth rate with increasing convective Mach number. When compressibility effects were included in the models the results showed a dramatic reduction in growth rate and peak values of the normalized Reynolds stress components with increasing convective Mach number. In addition, the results obtained using the new model for pressure-strain correlation gave improved agreement with the experimental data for normalized growth rate and peak values of the Reynolds stress components with increasing convective Mach number.

REFERENCES

1. Jones, W.P., and Launder, B.E., "The Prediction of Laminarization with a Two-Equation Model of Turbulence," International Journal of Heat and Mass Transfer, Vol. 15, 1972, pp. 301–314.

2. Launder, B.E., Reece, G.J., Rodi, W., "Progress in the Development of a Reynolds Stress Closure," Journal of Fluid Mechanics, Vol. 68, 1975, pp. 537–566.

3. Papamoschou, D., and Roshko, A., "The Compressible Turbulent Shear Layer: An Experimental Study," Journal of Fluid Mechanics, Vol. 197, 1988, pp. 453–477.

4. Elliott, G.S., and Samimy, M., "Compressibility Effects in Free Shear Layers," Physics of Fluids A, Vol. 2, 1990, pp. 1231–1240.

5. Oh, Y.H., "Analysis of Two-Dimensional Free Turbulent Mixing," AIAA 7th Fluid and Plasma Dynamics Conference, AIAA Paper No. 74–594, Palo Alto, Ca, June, 1974.

6. Vandromme, D., "Contribution a la modelization et la. Prediction D'ecoulements Turbulents a Masse Voluminque Variable," Sc.d Thesis, Universite Des Sciences et Techniques De Lille, France, September, 1983.

7. Dussauge, J.P., and Quine, C., "A Second-Order Closure for Supersonic Turbulent Flows : Application to the Supersonic Mixing," Proceedings of the Workshop on the Physics of Compressible Turbulent Mixing, Princeton, NJ, October, 1988.

8. Sarkar, S., Erlebacher, G., Hussaini, M.Y., and Kreiss, H.O., "The Analysis and Modelling of Dilatational Terms in Compressible Turbulence," Journal of Fluid Mechanics, Vol. 227, 1991, pp. 473–493.

9. Sarkar, S., "Modeling the Pressure-Dilatation Correlation," ICASE Report No. 91–42, NASA Langley Research Center, Hampton, Va, May, 1991.

10. Speziale, C.G., Sarkar, S., and Gatski, T.B., "Modeling the Pressure-Strain Correlation of Turbulence : An Invariant Dynamical Systems Approach," Journal of Fluid Mechanics, Vol. 227, 1991, pp. 245–272.

11. Sarkar, S., and Lakshmanan, B., "Application of a Reynolds Stress Turbulence Model to the Compressible Shear Layer," AIAA Journal, Vol. 29, 1991, pp. 743–749.

12. MacCormack, R.W., "The Effect of Viscosity in Hypervelocity Impact Cratering," AIAA Paper 69–534, Cincinnati, Ohio, April 1969.

13. Drummond, J.P., Rogers, R.C., and Hussaini, M.Y., "A Numerical Model for Supersonic Reacting Mixing Layers," Computer Methods in Applied Mechanics and Engineering, Vol. 64, 1987, pp. 39–60.

14. Carpenter, M.H., "The Effects of Finite Rate Chemical Processes on High Enthalpy Nozzle Performance: A Comparison between SPARK and SEAGULL," AIAA/ASME/SAE/ASEE 24th Joint Propulsion Conference, Boston, Massachusetts, July, 1988.

15. Kline, S.J., Cantwell, B.J., Lilley, G.M. (1980–1981) eds, AFOSR-HTTM-Stanford Conference, Vol. 1, Stanford University Press, Stanford, CA, 1982, pp. 368.

16. Petrie, H.L., Samimy, M., and Addy, A.L., "A Study of Compressible Turbulent Free Shear Layers using Laser Doppler Velocimetry," AIAA Paper 85–0177, January, 1985.

17. Ikawa, H., and Kubota, T., "Investigation of Supersonic Turbulent Mixing Layer with Zero Pressure Gradient," AIAA Journal, Vol. 13, May, 1975, pp. 566–572.

18. Wagner, R.D., "Mean Flow and Turbulence Measurements in a Mach 5 Free Shear Layer," NASA TN D-7366, December, 1973.

$$M_c = \frac{\Delta u}{a_1 + a_2}$$

$$\Delta u = u_1 - u_2$$

$$\eta = \frac{y - y_c}{\delta}$$

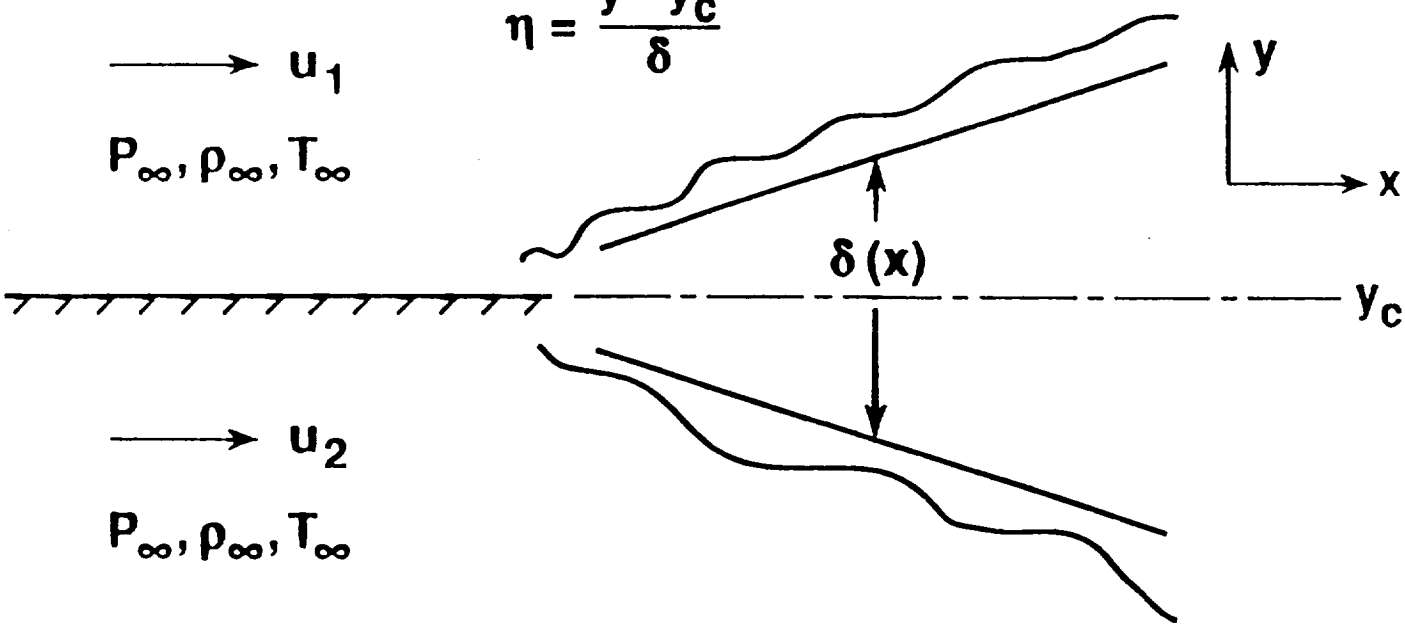

Fig. 2.1 Schematic of the compressible shear layer

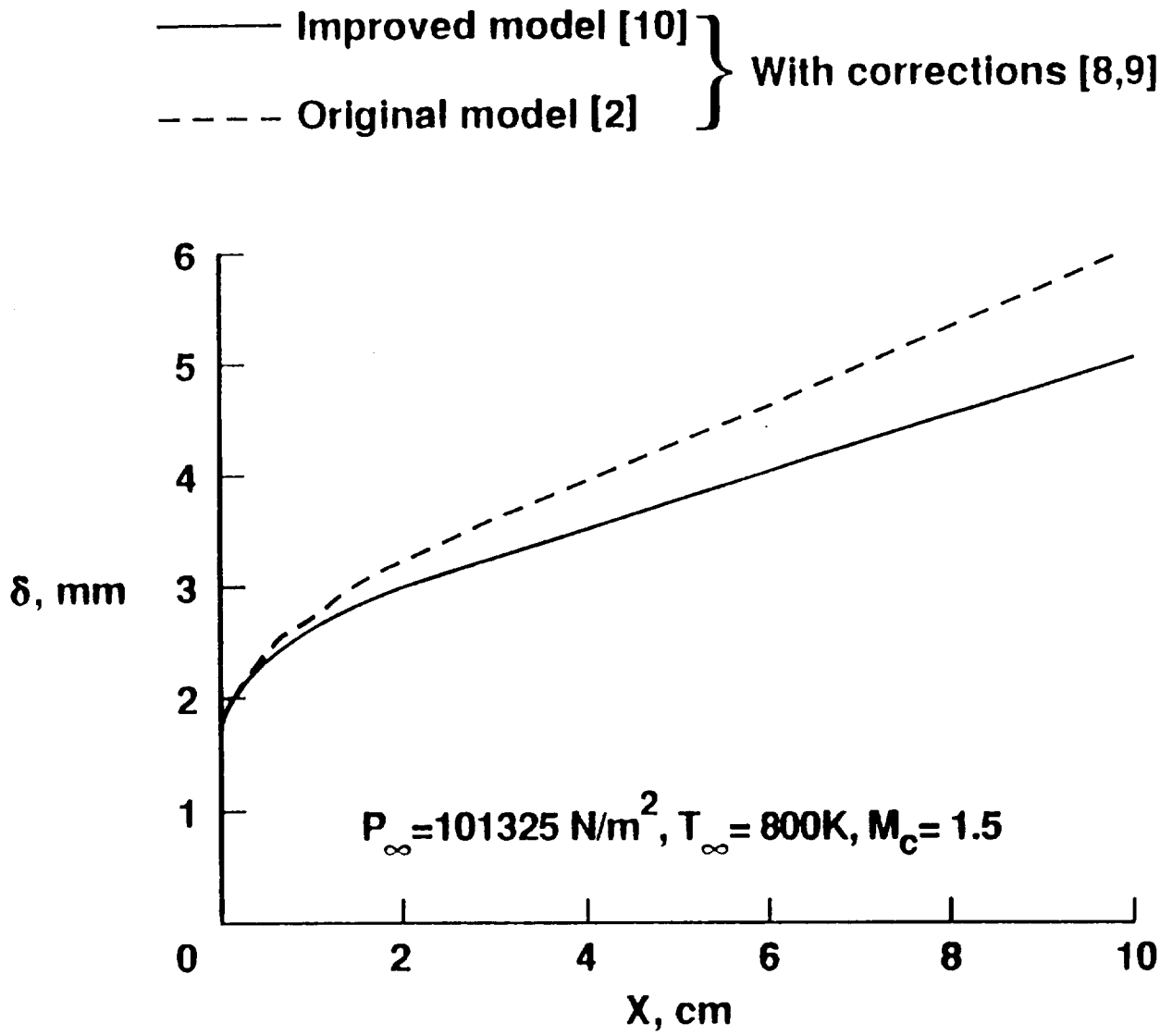

Fig. 4.1 Axial variation of the shear layer thickness

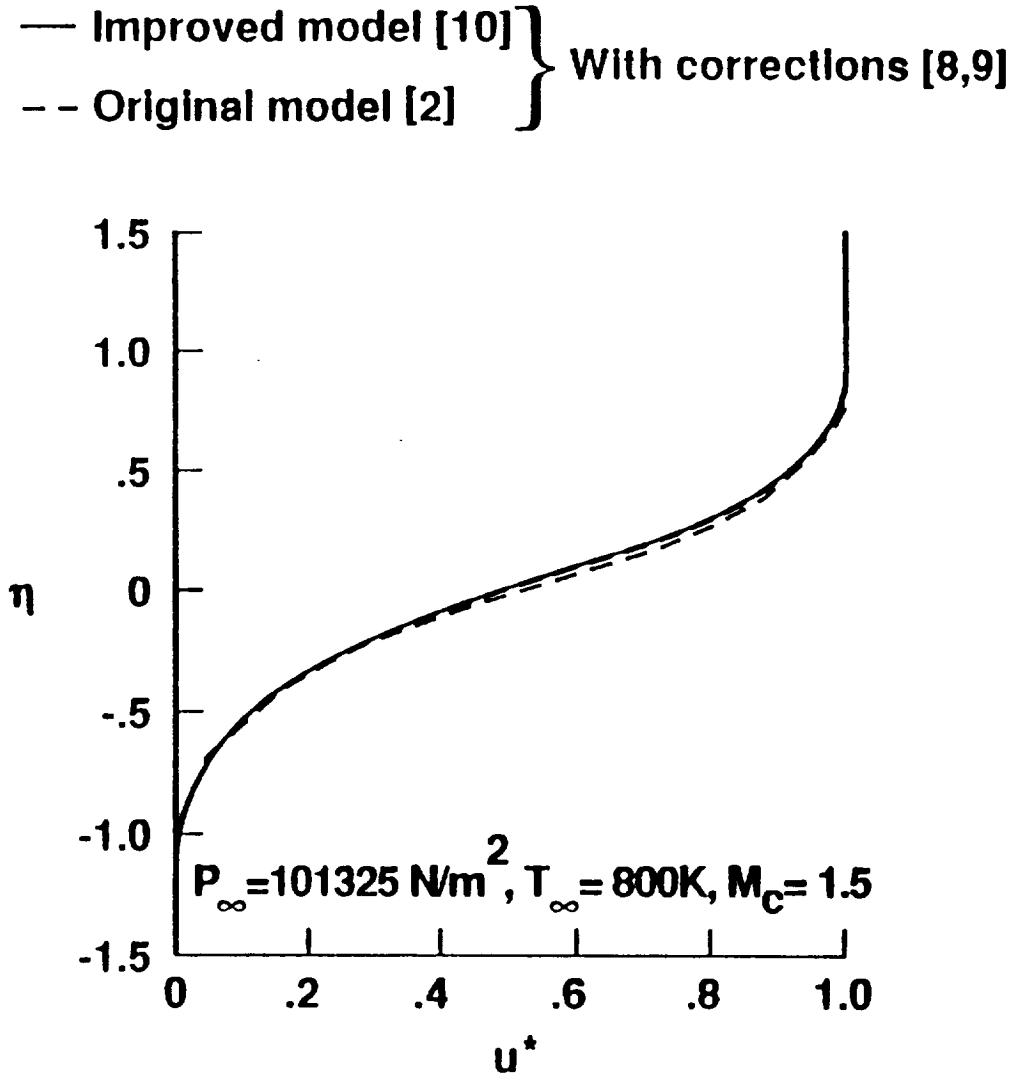

Fig. 4.2 Comparison of axial velocity profile at x = 10 cm

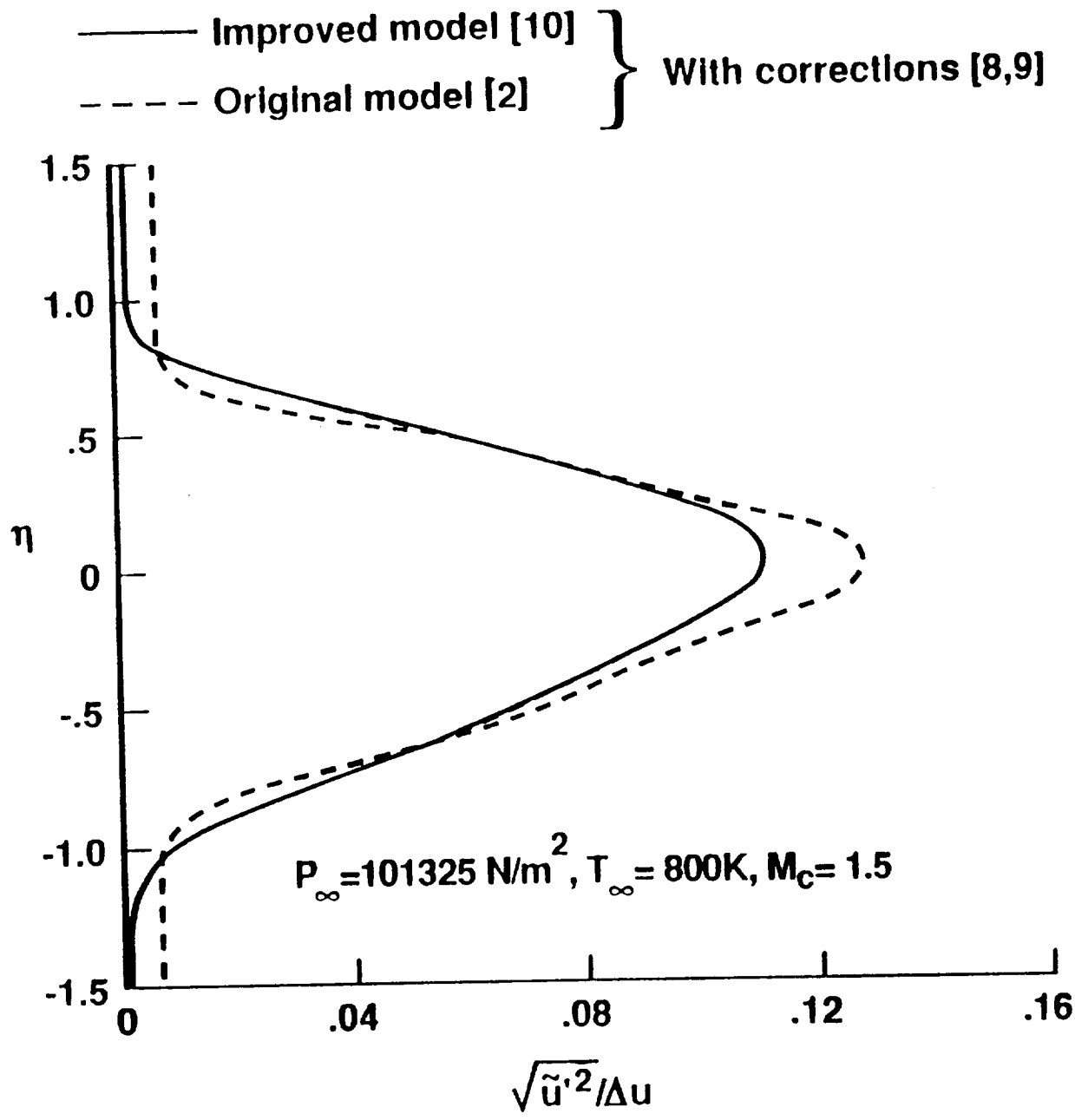

Fig. 4.3 Comparison of streamwise component of the Reynolds stress tensor at x = 10 cm

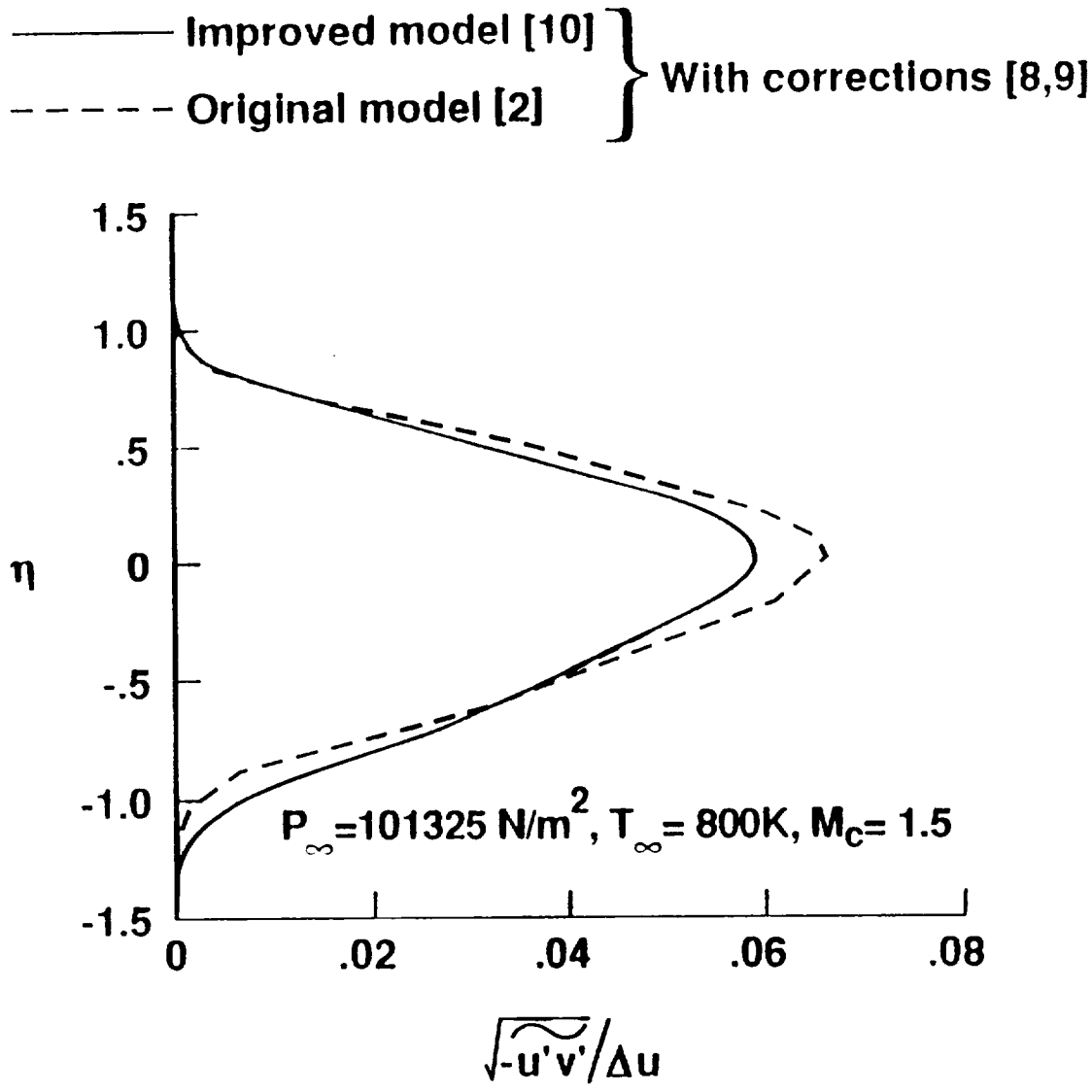

Fig. 4.4 Comparison of the Reynolds shear stress profile at x = 10 cm

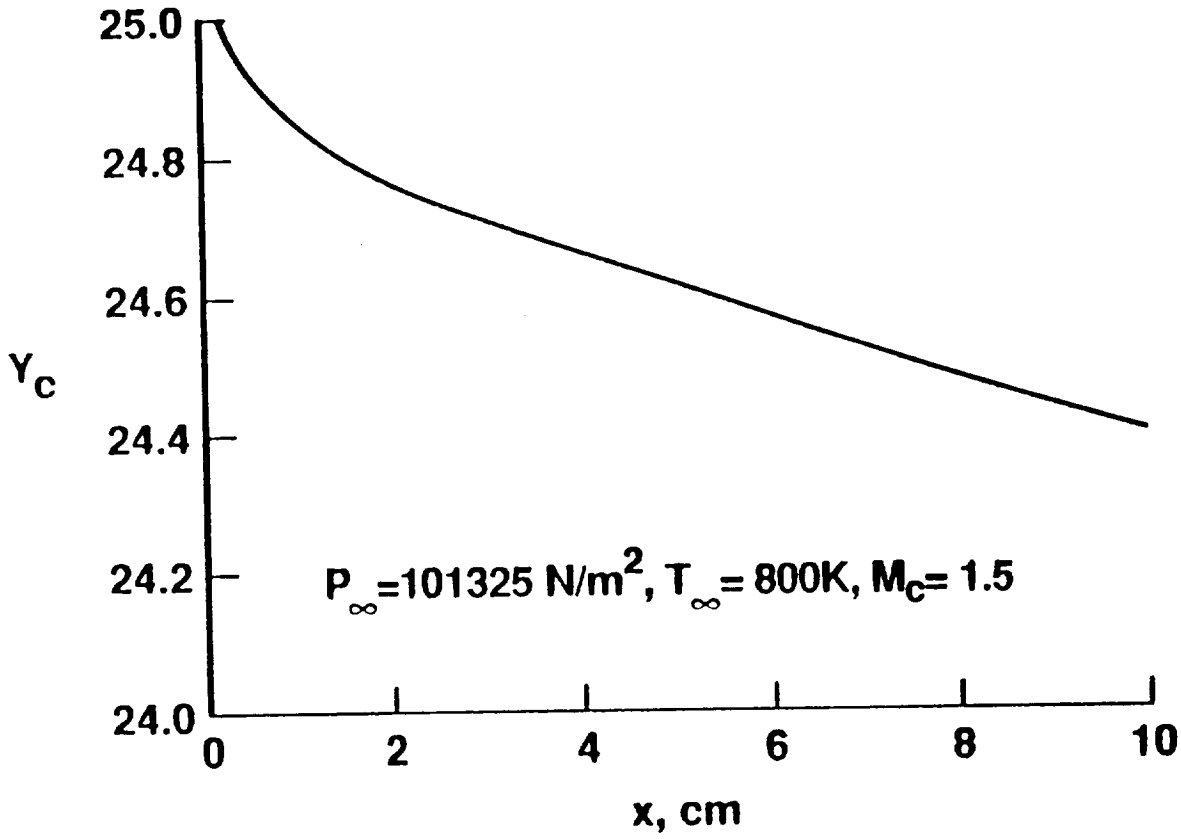

Fig. 4.5 Variation of the y coordinate location where $u^* = 0.5$ with axial location

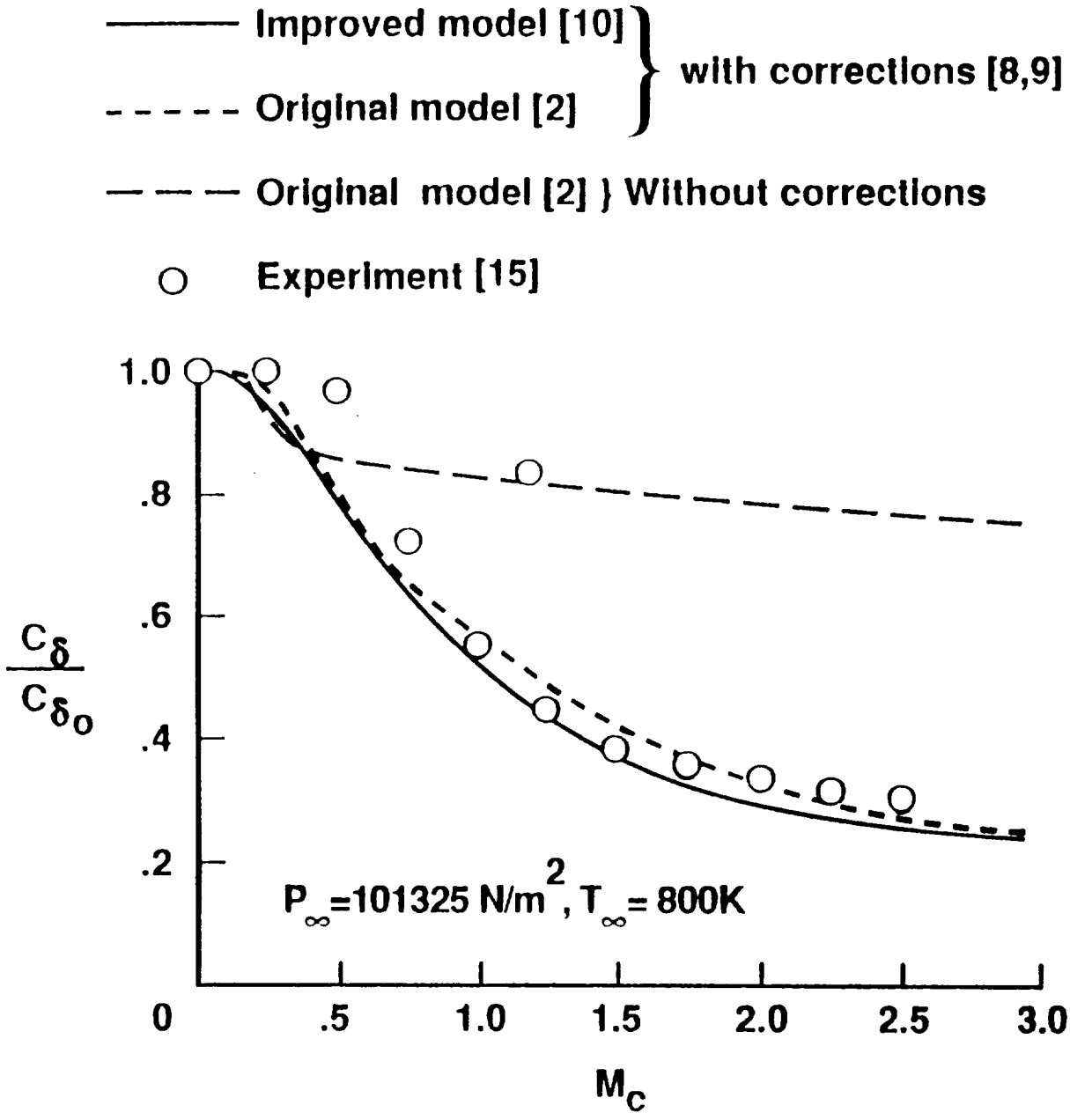

Fig. 4.6 Variation of the shear layer growth rate with the convective Mach number

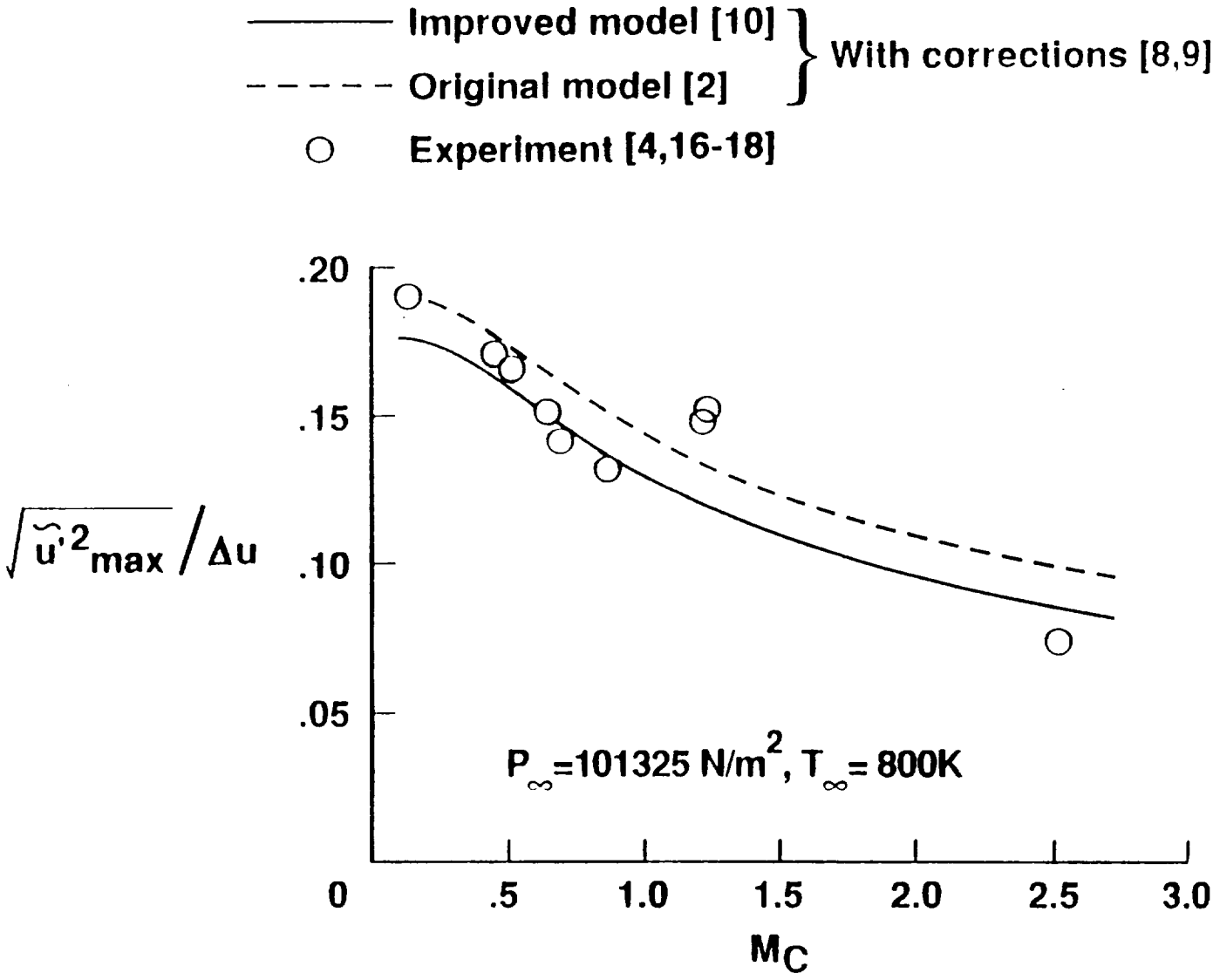

Fig. 4.7 Variation of the maximum streamwise stress with the convective Mach number

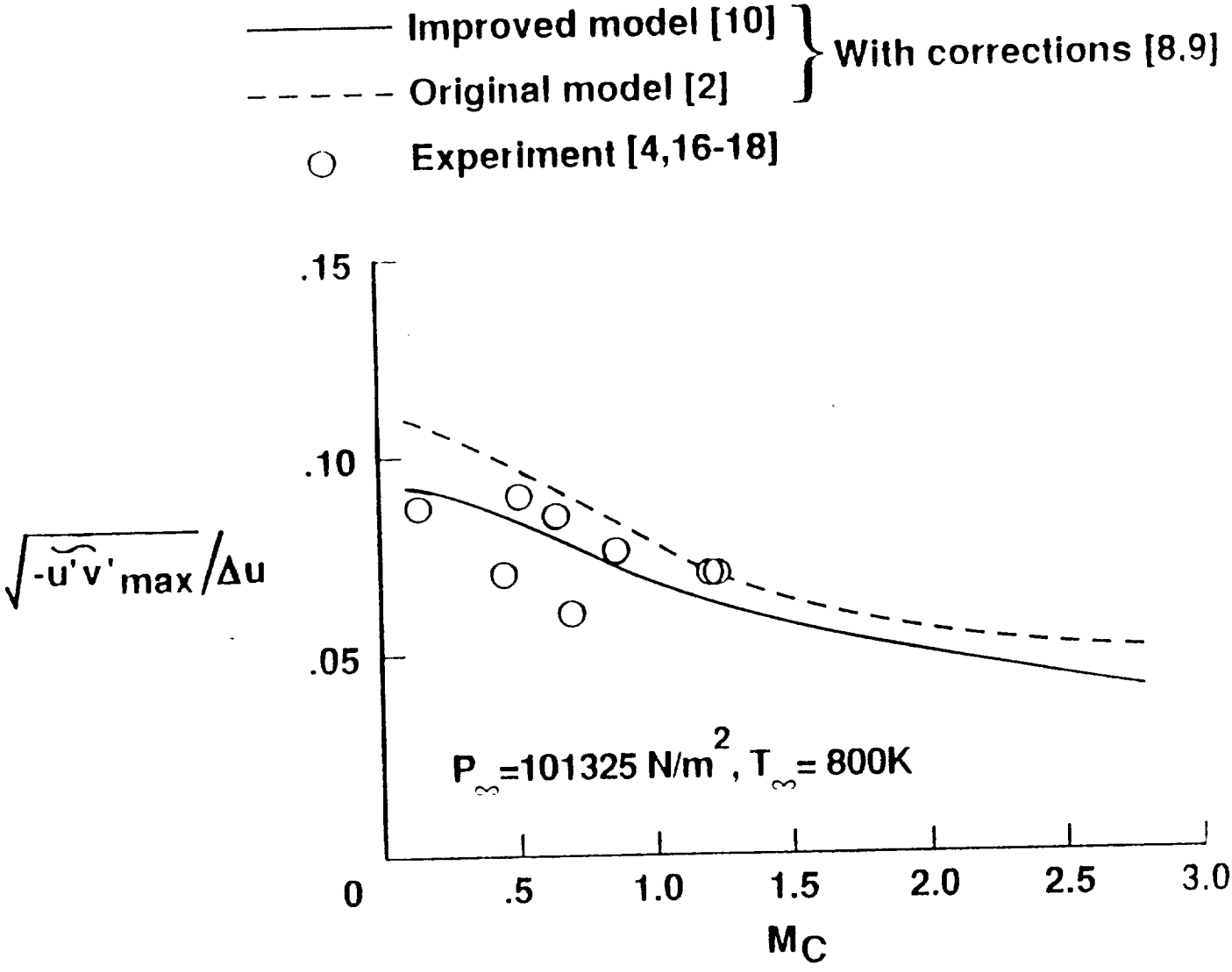

Fig. 4.8 Variation of the maximum Reynolds shear stress with the convective Mach number